JPE 17-5-19

https://doi.org/10.6113/JPE.2017.17.5.1317
ISSN(Print): 1598-2092 / ISSN(Online): 2093-4718

A Dynamic Power Distribution Strategy for Large-scale Cascaded Photovoltaic Systems

Kangan Wang*, Xiaojie Wu†, Fujin Deng**, and Feng Liu*

*,†School of Electrical and Power Engineering, China University of Mining and Technology, Xuzhou, China
**School of Electrical Engineering, Southeast University, Nanjing, China

Abstract

The cascaded H-bridge (CHB) multilevel converter is a promising topology for large-scale photovoltaic (PV) systems. The output voltage over-modulation derived by the inter-module active power imbalance is one of the key issues for CHB PV systems. This paper proposed a dynamic power distribution strategy to eliminate the over-modulation in a CHB PV system by suitably redistributing the reactive power among the inverter modules of the CHB PV system. The proposed strategy can effectively extend the operating region of the CHB PV system with a simple control algorithm and easy implementation. Simulation and experimental results carried out on a seven-level CHB grid-connected PV system are shown to validate the proposed strategy.

Key words: Cascaded H-bridge (CHB), Extended operating region, Grid-connected PV system, Power distribution, Power imbalance

I. INTRODUCTION

World-wide renewable energy resources, especially solar energy, have grown dramatically in recent years, which is driven by a reduction in PV system prices and various national policies promoting the use of renewable energy [1], [2]. Multi-MW large-scale PV power plants, which play an important role in the development of PV systems, have seen a continuation in this upward trend [3].

The cascaded H-bridge multilevel converter is considered to be one of the most suitable configurations for large-scale PV power plants thanks to its modularity, scalability and distributed maximum power point trancking (DMPPT) [4]-[6]. When compared to conventional PV central inverters, the CHB inverters can generate three-phase medium-voltage (MV) multilevel voltage waveforms that do not require harmonic filters or set-up transformers [7].

When cascaded H-bridge multilevel converters are applied to large-scale PV systems, the inter-phase power imbalance and inter-module power imbalance caused by shading, dirt, temperature inhomogeneity, faulty H-bridges, aging and manufacturing tolerances [8], are ones of the important issues. Unbalanced power generation among the three phases causes unbalanced grid current, which can be addressed by means of control strategies and topologies [9], [10].

Regarding inter-module power imbalance, several technical papers have proposed a number of methods [11]-[15]. In [11], an energy-balance control strategy is presented to achieve the maximum energy harvest. Reference [12] proposes a mixed staircase-PWM technique in CHB PV systems, which can decrease the switching frequency and increase the power extraction. Methods including n voltage control loops in [13] and [14] are implemented to control each of the dc-link voltages by manipulating the modulation index of each inverter module in single-phase and three-phase CHB PV systems. However, the procedure for controller design is not generalized to higher levels, since the control structure is more complex for higher levels and the design analysis is more difficult. An improved control strategy that consists of only one total voltage loop and n feed-forward-based weighting factors is proposed in [15], where the weighting factors is generated by the DC link input powers and voltage references. Therefore, the control strategies are independent from the output of the voltage feedback loop which simplifies the control structures in [13], [14].

Manuscript received Sep. 4, 2016; accepted May 30, 2017
Recommended for publication by Associate Editor Alian Chen.
†Corresponding Author: zgcumt@126.com
Tel: +86 516 83592130, China University of Mining and Technology
*School of Electrical and Power Engineering, China University of Mining and Technology, China
**School of Electrical Engineering, Southeast University, China

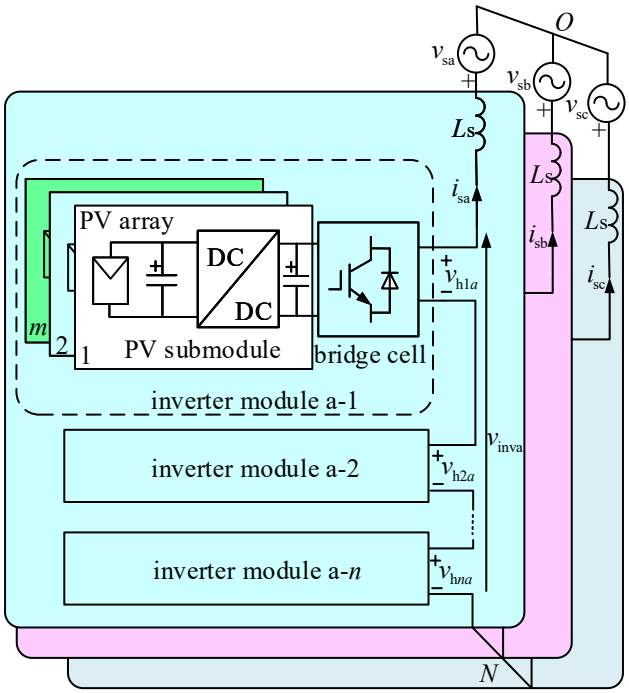

Fig. 1. Diagram of a three-phase CHB PV system.

However, the disadvantages of these methods are that they have not presented a quantitative evaluation of the stable operation range, and they have not proposed an effective strategy to mitigate the over-modulation issue caused by a severe inter-module power imbalance, which can result in system instability and distorted grid current.

Reference [16] proposes a method where the control system reduces the power of inverter modules to avoid over-modulation. The technique is capable of stabilizing systems under imbalanced condition. However, it results in a lower output power and a less-efficient system.

In reference [17], a hybrid modulation is used along with a derivative-of-power-based control method to utilize CHB cells up to their full potential and to stabilize single-stage cascaded H-bridge inverters under severe mismatching conditions. However, the system is based on dP/dI, which is noise sensitive.

One of the most-commonly referred methods for mitigating the over-modulation in CHB PV systems is based on a reactive power compensation algorithm (RPCA), which helps MPPT implementation and significantly improves system reliability. However, the reactive power is limited in consideration of the system capacity and power factor. In [18], [19], a power allocation principle was presented to optimize the reactive power allocation among inverter modules. Unfortunately, this method has to establish the grid-connected current coordinate frame and calculate the reactive power allocation coefficient in advance, which is both complex and inflexible.

The aim of this paper is to optimize the reactive power distribution and to mitigate over-modulation for large-scale cascaded PV systems. A quantitative evaluation of the stable operation range with imbalanced power generation is presented. When over-modulation occurs, RPCA is activated and RPRA redistributes the reactive power among the inverter modules by the regulation of the q-axis components, which is characterized by easy implementation and flexibility. In addition, the application range of the proposed strategy is analyzed.

This paper is organized as follows. In section II, a cascaded PV system configuration is presented and a quantitative analysis of the inter-module active imbalance is obtained. In section III, the proposed strategy is illustrated. A 3MW PV system including three cascaded inverter modules in each phase with the proposed control strategy is modeled in MATLAB/Simulink and a PV system prototype has been built in the laboratory. Simulation and experimental results are presented to verify the validity of the control strategy in sections IV and V. Finally, some conclusions are presented in section VI.

II. Analysis of CHB PV Systems

A. System Configuration

Fig. 1 shows a diagram of a three-phase CHB PV system, where each phase is composed of n series-connected inverter modules and an arm inductor L_s. Each inverter module consists of one bridge cell and m parallel-connected PV submodules where PV arrays are connected to the dc link of the bridge cell via DC/DC converters. A DC/DC converter with a high frequency transformer is used for galvanic isolation between the PV arrays and the MV grid, which is required because most commercial PV modules can withstand no more than 1000V between the active part and the grounded frame [20]. On the other hand, DC/DC converters decouple the second-harmonic voltage ripple between the input voltages of the bridge cell and DC/DC converters [9], which helps the MPPT implementation. This paper makes no constrains on the isolated DC/DC converters to be employed. Several literatures have presented a few of circuit configurations for this application [21], [22], whose behavior can be considered as a dc power source.

The n bridge cells are connected in series in each phase. The output voltage of each bridge cell is denoted as v_{hip}, which can synthesize a $2n$+1 level inverter output voltage v_{invp} (i=1,… n and p=a, b, c). v_{sp} and i_{sp} represent the grid voltage and current, respectively. The dc-link voltage of each bridge cell is regulated to V_{dc}, which means the inflow of energy from the PV submodules is equal to the outflow of energy of the bridge cells.

In each phase, the gird voltage vector $\mathbf{V_{sp}}$, the grid current vector $\mathbf{I_{sp}}$, and the inverter output voltage vector $\mathbf{V_{invp}}$ can be expressed as:

$$\mathbf{V_{invp}} = j\omega L_s \mathbf{I_{sp}} + \mathbf{V_{sp}} \quad (1)$$

where ω denotes the system fundamental frequency.

Given the relationship of the inverter output voltage vector $\mathbf{V_{invp}}$ and the output voltage vector of each inverter module $\mathbf{V_{h}}_{i}\mathbf{_p}$, (1) can also be expressed as:

$$\sum_{i=1}^{n} \mathbf{V_{h}}_{i}\mathbf{_p} = j\omega L_s \mathbf{I_{sp}} + \mathbf{V_{sp}} \quad (2)$$

B. Control System

The cascaded PV control system for Phase A based on the d-q coordinate frame is depicted in Fig. 2, where the d-q coordinate frame is established by referring to [23] and T is the single-phase frame transformation matrix. The control system mainly consists of three parts: (a) the active and reactive current references; (b) the feedforward decoupling control structure; (c) the modulation waveform references.

The power reference of the ith bridge cell p_i^* is obtained by comparing the measured dc-link voltage v_{dci} with the command reference V_{dc}. The phase power reference p^* is obtained by summing the n power references. The active current reference i_d^* is the ratio of the phase power reference and the grid voltage amplitude V_{sa}.

The average d-axis and q-axis duty cycles d_d^* and d_q^* are obtained by comparing the inverter output voltage references to nV_{dc}. To achieve the maximum energy harvest in the unbalanced condition, the d-axis duty cycle needs to be modified and the compensating d-axis duty cycle of the ith inverter module in Phase A can be expressed as:

$$\Delta d_{di}^* = K_{\Delta d}(\bar{v}_{dc} - v_{dci}) \quad (3)$$

where $\bar{v}_{dc}$ is the dc-link mean voltage in Phase A. $K_{\Delta d}$ is a proportional controller.

When the modified d-axis duty cycle d_{di}^* and the average q-axis duty cycle d_q^* are determined, the modulation waveform s_i is obtained by the inverse matrix T^{-1}.

C. Over-Modulation

In a real system, due to shading, dirt, temperature inhomogeneity, faulty H-bridges, aging and manufacturing tolerances, active power imbalances occur and result in over-modulation, which is illustrated in Fig. 3.

According to the control system in Fig. 2, when each inverter module is in its rated condition and generates a balanced active power P_r, the system operates with a unity power factor, where the total power in Phase A is denoted as P_a. The voltage distribution of n cascaded inverter modules in the d-q coordinate frame is shown in Fig. 3(a). Note that the voltage drop of the filter inductor is illustrated to be oversized for better understanding.

The d-axis components and the q-axis components of the output voltages of the inverter modules are equal. According to (2), the corresponding duty cycles are uniform (d_{d1}=…=d_{dn}=d_d and d_{q1}=…=d_{qn}=d_q) and can be derived by:

$$\sum_{i=1}^{n} V_{dc} d_d = V_{sa} \quad (4)$$

$$\sum_{i=1}^{n} V_{dc} d_q = \omega L_s I_{da} \quad (5)$$

where I_{da}=$2P_a/V_{sa}$ is the magnitude of the grid current vector $\mathbf{I_{da}}$.

When a cascaded PV system works with slightly imbalanced active power generation, as shown in Fig. 3(b), the system maintains stable operation with a unity power factor. The d-axis duty cycle $d_{di}^{(u)}$ and the q-axis duty cycle $d_{qi}^{(u)}$ of the ith inverter module can be derived by:

$$\sum_{i=1}^{n} V_{dc} d_{di}^{(u)} = V_{sa} \quad (6)$$

$$\sum_{i=1}^{n} V_{dc} d_{qi}^{(u)} = \omega L_s I_{da}^{(u)} \quad (7)$$

where $I_{da}^{(u)}$ is the magnitude of the grid current in the unbalanced condition.

For the subsequent analysis, a set of ratios λ_1, λ_2 … λ_n to describe the active power of the ith inverter module P_i with respect to P_r is introduced:

$$\lambda_i = \frac{P_i}{P_r} \quad (8)$$

The grid current is a result of the power transformed to the grid from all the inverter modules, so the current magnitude is equal to $\sum_{i=1}^{n} \lambda_i I_{da}/n$ in an unbalanced condition. The current flowing through the inverter modules in Phase A is the same, and the d-axis component $d_{di}^{(u)}$ can be derived from a point of power by:

$$\frac{P_i}{P_r} = \frac{I_{da}^{(u)}}{I_{da}} \cdot \frac{d_{di}^{(u)}}{d_d} \quad (9)$$

According to (4), (6), (8) and (9), $d_{di}^{(u)}$ can be calculated as:

$$d_{di}^{(u)} = \frac{\lambda_i V_{sa}}{\sum_{l=1}^{n} \lambda_l V_{dc}} \quad (10)$$

The reactive power is equally distributed among the inverter modules according to the control system. Based on (5), (7) and (8), $d_{qi}^{(u)}$ can be derived as:

$$d_{qi}^{(u)} = \frac{\omega L_s I_{da} \sum_{l=1}^{n} \lambda_l}{n^2 V_{dc}} = \frac{2\omega L_s P_a \sum_{l=1}^{n} \lambda_l}{n^2 V_{dc} V_{sa}} \quad (11)$$

Considering the limitation of the modulation index, the ith inverter module should be subject to the constraint shown in (12). It can be seen that in order to avoid over-modulation, the inter-module active power imbalance is limited. The same analysis can be applied in Phase B and Phase C.

$$\sqrt{\left(\frac{\lambda_i V_{sa}}{\sum_{l=1}^{n} \lambda_l V_{dc}}\right)^2 + \left(\frac{2\omega L_s P_a \sum_{l=1}^{n} \lambda_l}{n^2 V_{dc} V_{sa}}\right)^2} \le 1 \quad (12)$$

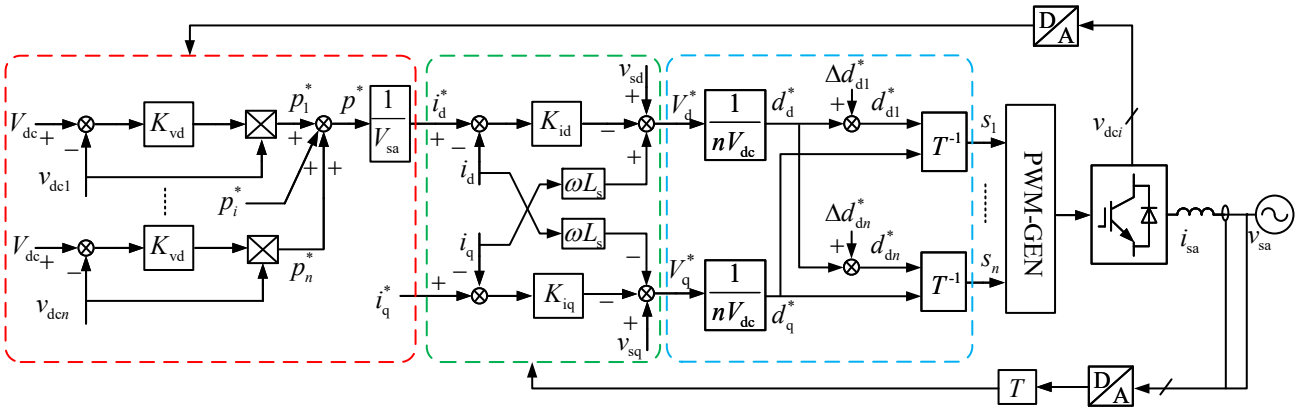

Fig. 2. Cascaded PV Control diagram for Phase A based on the d-q coordinate frame.

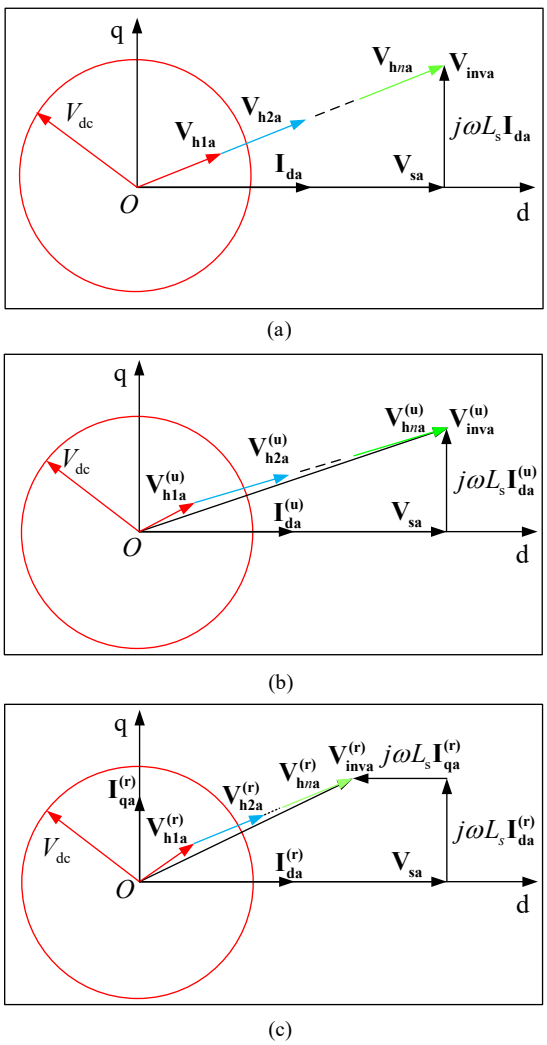

Fig. 3. Voltage distribution of n cascaded inverter modules in the d-q coordinate frame: (a) with balanced active power generation; (b) with imbalanced active power generation; (c) with RPCA in the unbalanced condition.

III. The Proposed Control Strategy

During system operation, an active power imbalance may occur and cause over-modulation, especially for inverter modules with a higher active power output. Once the over-modulation is identified, the reactive power compensation algorithm (RPCA) is activated. The amplitude of the reactive current reference I_q^* is given by:

$$I_q^* = \mu I_d^* \tag{13}$$

where I_d^* is the amplitude of the active current reference, and μ is the reactive current factor.

The voltage distribution of n cascaded inverter modules in Phase A with RPCA is shown in Fig. 3(c). The d-axis output voltage of the invert modules decreases $\omega L_s I_{qa}^{(r)}$, where $I_{qa}^{(r)}$ is the amplitude of the reactive current with RPCA. However, an AC inductor sized at about 5% with respect to nominal conditions can be regarded as sufficient for the ac link buffer and current control [7], and the system capacity is limited. Therefore, the capacity of RPCA to eliminate over-modulation is limited. RPRA redistributes the reactive power among the inverter modules, which promotes the capacity for eliminating over-modulation and extends the system operation range. The operation principle of RPRA is explained in the following paragraphs.

A. RPRA

RPRA is achieved by regulating the q-axis duty cycles of the inverter modules in the control system shown in Fig. 2, which is depicted in Fig. 4. The modified q-axis duty cycle d_{qi}^* is obtained by adding the average q-axis duty cycle d_q^* and the compensating q-axis duty cycle Δd_{qi}^*. RPRA is achieved by the following steps: 1) calculate the modulation waveform amplitude S_i; 2) sort S_i in ascending order; 3) combine two inverter modules according to the sorting result and redistribute the q-axis duty cycles among the inverter modules. Fig. 5(a) shows a flowchart of RPRA.

Due to the inputs in Fig. 5(a), the modulation waveform amplitude S_i is easily obtained in the d-q coordinate frame and can be calculated by:

$$S_i = \sqrt{(d_d^* + \Delta d_{di}^*)^2 + (d_q^* + \Delta d_{qi}^*)} \tag{14}$$

S_i is sorted in ascending order. Bear in mind that the index

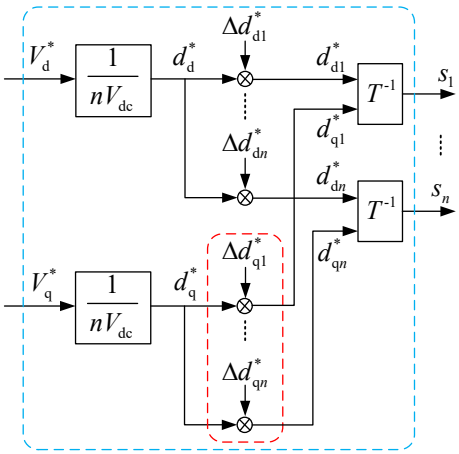

Fig. 4. The block diagram of RPRA.

i indicates the inverter module position in the physical circuit while Lu (u=1,…,x) and Hv (v=1,…,y) represent the ordering index after sorting where value of S_i less than 1 is x, and the value greater than 1 is y.

According to the sorting result, the inverter module with the ordering index Lj and the other inverter module with the ordering index $H(y\text{-}j\text{+}1)$ form a combination C_j (j=1,…x or y). The combining principle is that the greater the modulation waveform amplitude of one inverter module, the less the other one is in a combination, such as C_1 { S_{L1} , S_{Hy} }, C_2{ S_{L2} , $S_{H(y\text{-}1)}$ } and so on. The inverter module in the physical circuit, which corresponds to $S_{H(y\text{-}j+1)}$ in C_j, needs to subtract Δd_{qHj}^* if i_q^* is negative and add Δd_{qHj}^* if i_q^* is positive in the q-axis duty cycle. The other inverter module in the physical circuit, which corresponds to S_{Lj} in C_j, needs to add Δd_{qj}^* and subtract Δd_{qj}^*, where:

$$\Delta d_{qHj}^* = K_{\Delta q}(S_{H(y\text{-}j+1)}\text{-}1) \tag{15}$$

where $K_{\Delta q}$ is a PI controller.

In the control strategy, the time constant for obtaining the compensating q-axis duty cycle Δd_{qi}^* is much larger than that for the compensating d-axis components. When the active power P_i is fixed, the d-axis duty cycles adjust automatically according to the modified q-axis duty cycles. Therefore, the disturbances to Δd_{di}^* are insignificant. The output of the voltage control loops V_d^* and V_q^* are not be disturbed because in the combination C_i, the inverter module with the ordering index Lj adds Δd_{qj}^* and the other inverter module with the ordering index $H(y\text{-}j\text{+}1)$ subtracts Δd_{qj}^*, which ensures that the upper layers of the control system are kept stable.

In this example, S_1 corresponds to the ordering index $L2$ and is equal to S_{L2}. In part of the combination, the inverter module with ordering index $H2$ and the other one with $L1$ form combination C_1. According to the combining principle, C_2 is also confirmed and the inverter module corresponding to $L3$ is left, which waits to be sorted in the next control period. After the combination, the q-axis duty cycle for the inverter module with the ordering index $H2$ in C_1 needs to add Δd_{qH1}^*, which is obtained by (15), and the q-axis duty cycle for the inverter module with ordering index $L1$ in C_1 needs to subtract Δd_{qH1}^*. The q-axis duty cycles of the inverter modules in C_2 are similar to those in C_1, which determine the modified q-axis duty cycles.

B. Evaluation of the Adjusting Ability

The proposed strategy is applicable within a certain region and the ability for eliminating over-modulation is limited. The output power of the ith inverter module can be expressed as:

$$\lambda_i P_r = \frac{3}{2}(I_d^* \cdot V_{dc} \cdot d_{di}^{(d)} + \mu I_d^* \cdot V_{dc} \cdot d_{qi}^{(d)}) \tag{16}$$

where $d_{di}^{(d)}$ and $d_{qi}^{(d)}$ denote the d-axis and q-axis duty cycles

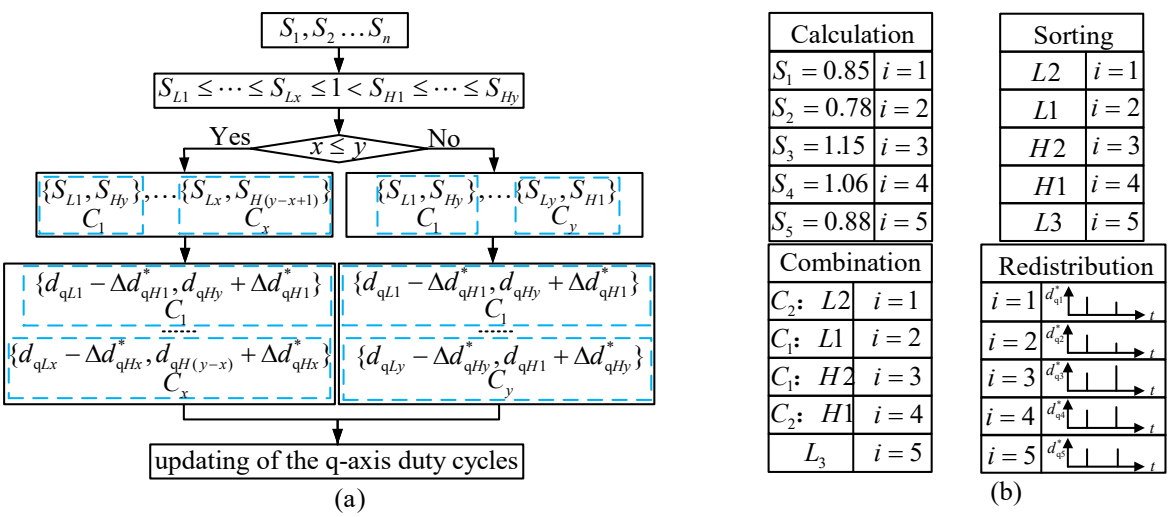

Fig. 5. (a) Flowchart of RPRA (assuming i_q^*>0) and (b) redistribution process in the case of n=5.

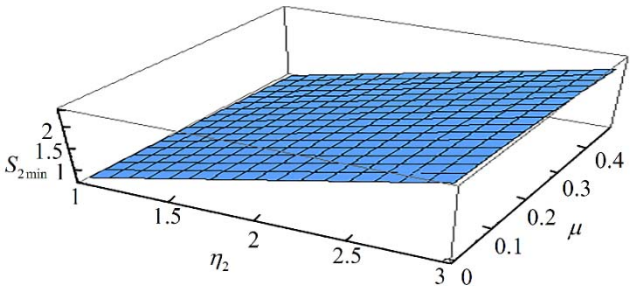

Fig. 6. Relationship between S_{2min}, $\eta_2$and μ (d_d=0.78 and i_q^*>0).

after power redistribution. The relationship between $d_{di}^{(d)}$ and $d_{qi}^{(d)}$ can be derived from (4), (8) and (16) as:

$$d_{di}^{(d)} + \mu d_{qi}^{(d)} = \frac{n\lambda_i}{\sum_{l=1}^{n}\lambda_l} \cdot \frac{V_{sa}}{nV_{dc}} \tag{17}$$

An indicator of the inter-bridge power imbalance for the ith module η_i is defined as:

$$\eta_i = \frac{\lambda_i}{\frac{1}{n}\sum_{l=1}^{n}\lambda_l} \tag{18}$$

Therefore, (17) can also be expressed as:

$$d_{di}^{(d)} + \mu d_{qi}^{(d)} = \frac{\eta_i V_{sa}}{nV_{dc}} \tag{19}$$

If the reactive current factor μ and η_i are confirmed, the minimum value of S_i S_{imin} can be derived by:

$$\frac{d}{d(d_{di}^{(d)})} S_i(d_{di}^{(d)}, d_{qi}^{(d)}) = 0 \tag{20}$$

where $d_{qi}^{(d)}$ can be expressed by $d_{di}^{(d)}$.

In order to eliminate over-modulation, S_{imin} must be less than 1 by adjusting μ and η_i. Take n=3 as an example for clarity and assume that $\lambda_1<\lambda_3<\lambda_2$. Then the relationship between S_{2min}, η_2 and μ is shown in Fig. 6. It can be seen that S_{2min} decreases with the increasing of μ and that it increases with the increasing of η_2. If S_{2min} is always greater than 1 with a certain μ, the proposed strategy cannot eliminate over-modulation.

IV. Simulation Results

The proposed control strategy for grid-connected cascaded PV system is validated in MATLAB/Simulink. The parameters of the seven-level CHB PV system are listed in Table I. The dc-link voltage of each bridge cell was regulated to 2000V. The single PV module which reaches a nominal peak power of 305W at the MPP is constructed in MATLAB/Simulink. Each bridge cell is fed by 15×72 PV modules by DC/DC converters. Fig. 7 shows the d-axis and q-axis grid current during the whole system operation. During the period of 0.3~t_1, each inverter module operates under the rated symmetrical condition of 1000W/m^2 and 25℃, and the

TABLE I
SIMULATION SYSTEM CIRCUIT PARAMETERS

Parameters	Symbols	Values
Grid Voltage	V_{sa}	4.89kV
Nominal Power	P_a	1MW
AC voltage frequency	f	50Hz
Filtering Inductor	L_s	3.3mH
Equivalent Resistor	R_s	0.2Ω
Capacitance Size	C_i	3.3mF
Number	n	3
Switching Frequency	f_{sw}	5kHz

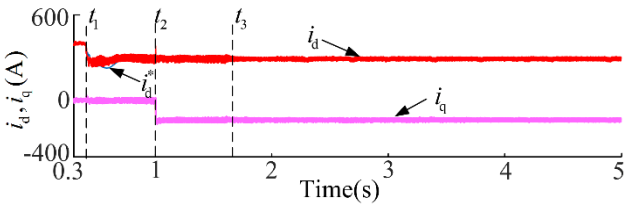

Fig. 7. d-axis and q-axis grid current waveforms of Phase A for a CHB grid-connect PV system.

MPPT is enabled and is implemented by DC/DC converters. The grid current i_{sa}, dc-link voltage v_{dci}, converter output voltage v_{inva} and d-axis duty cycle for the three inverter modules d_{di} over five periods is shown in Fig. 8, where a unity power factor is implemented and the grid current THD is 1.63%.

At t_1, the first module works at 700W/m^2 and 25℃, and the third module works at 600W/m^2 and 25℃ ($\lambda_3<\lambda_1<\lambda_2\leq1$). According to the previous analysis, the second inverter module carries a greater proportion of the whole ac output voltage, leading to over-modulation. The distorted current i_{sa} and the output voltage of the second module v_{h2a} are shown in Fig. 9. In this case, the harmonic distortion is 5.27%. RPCA with i_q^*=-140A is embed in the control system at the moment of t_2, where the positive direction of the grid current in Simulink is contrary to that in Fig. 1. The capacity to eliminate over-modulation is limited with only RPCA and the second inverter module still operates with over-modulation. At t_3, RPRA is activated. Through the sorting algorithm and the combination during each control period, the q-axis duty cycles are redistributed until S_2 is equal to 1.

During the dynamic adjusting process, the d-axis duty cycle of the second bridge cell decreases and that of the first and third bridge cells increase correspondingly, as shown in Fig. 10. In this case, the harmonic distortion decreases to 2.38% and the chosen inverter module index to form the combination C_1 M_{min} with a maximum modulation amplitude changes from 1 to 3 and M_{max} with a maximum modulation amplitude is 2. Fig. 11 presents the dynamic adjusting process, where the modulation waveform amplitude of the second bridge cell S_2 gradually decreases to 1 and the

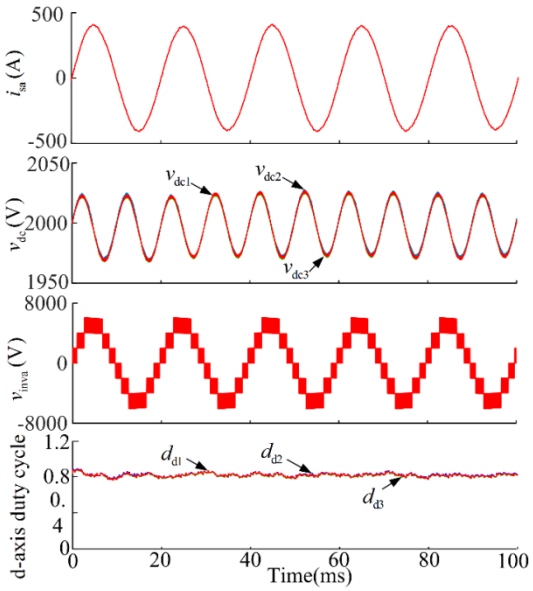

Fig. 8. Simulation results for the grid current i_{sa}, dc-link voltage $v_{dc1,2,3}$, converter output voltage v_{inva} and d-axis duty cycle for three inverter modules $d_{d1,2,3}$ over five periods under balanced power conditions.

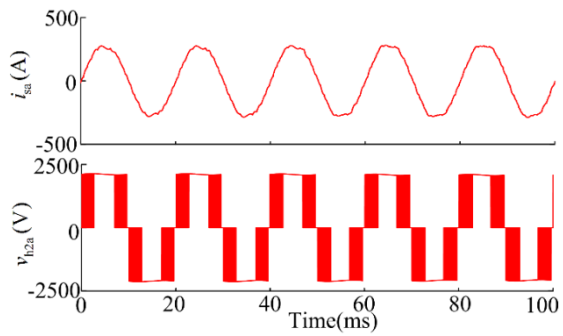

Fig. 9. Simulation results for the distorted current i_{sa} and the PWM output voltage of the second module v_{h2a} under imbalanced power conditions without the proposed strategy.

modulation waveform amplitudes of the first and third bridge cells increase correspondingly.

In (15), the reference value is 1 so that the modulation index of the second inverter module after the redistribution cannot be lower than 1. When moderately decreasing the reference value, the redistribution can be carried out at a greater depth.

V. Experimental Results

To verify the feasibility of the proposed strategy, a single-phase 1kW CHB PV system was built and connected to the grid as shown in Fig. 12. The parameters of the test system are listed in Table II. The prototype is not equipped with DC/DC converters, which has no effect the results of this paper, as long as an inter-module power imbalance is created. Each PV simulator generates 360W of active power under its rated condition and each dc-link voltage is regulated

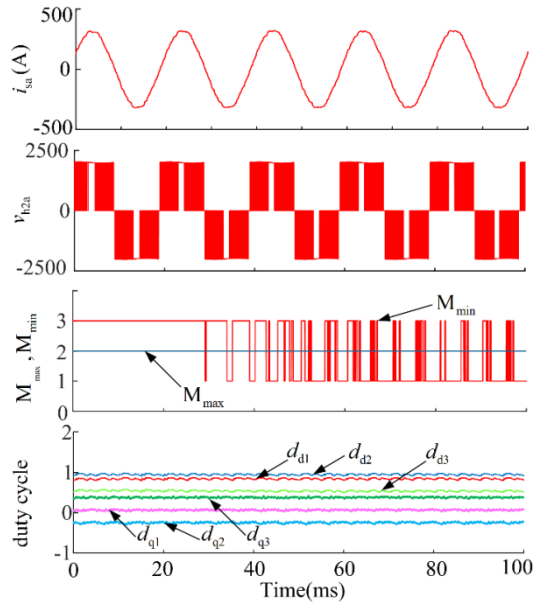

Fig. 10. Simulation results for the distorted current i_{sa}, the PWM output voltage of the second module v_{h2a}, the chosen inverter module index to form the combination C_1 M_{min} and M_{max} and the d-axis and q-axis components of the three modulation waveforms under imbalanced power conditions with the proposed strategy.

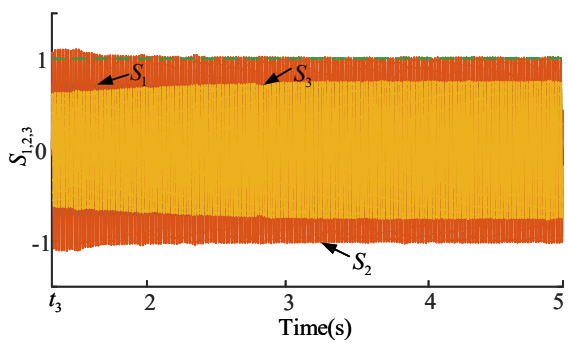

Fig. 11. Modulation waveforms of three bridge cells with the proposed strategy during the dynamic adjusting process.

TABLE II
Experimental System Circuit Parameters

Parameters	Symbols	Values
Grid Voltage	V_{sa}	141V
Nominal Power	P_a	1kW
AC Voltage Frequency	f	50Hz
Filtering Inductor	L_s	5mH
Capacitor Size	C_i	3.3mF
Cascaded Number	n	3
Switching Frequency	f_{sw}	5kHz

to 60V. The system is connected to the grid through a transformer and the peak voltage of the secondary side is regulated to 141V. The control platform consists of one master controller and three slave controllers. The master controller contains one DSP and one FPGA, and each slave controller has one FPGA, which is shown in Fig. 13.

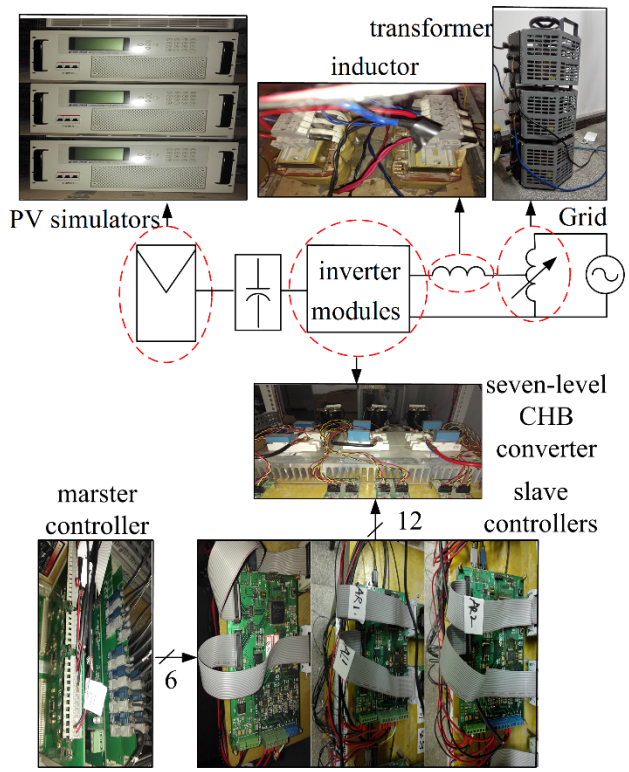

Fig. 12. Experimental setup and controllers.

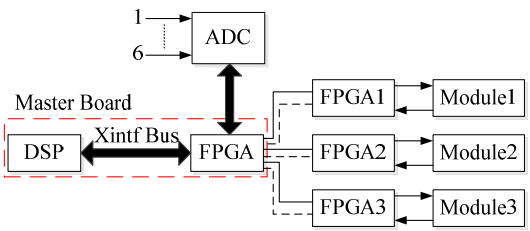

Fig. 13. Block diagram of the controllers in the experiment.

Fig. 14 shows experimental waveforms with balanced power generation. The THD of the output current is 3.5%. The current is in phase with the grid voltage which means a unity power factor. This experimental system uses IGBTs rated at 1200V and 50A. The semiconductor voltage drop and dead-time have a bad effect on the grid current. In addition, the grid voltage is distorted with a THD of 2.3% and the low-frequency transformer is not ideal. All of the three dc-link voltages in Fig. 14(b) have been set as 60V with a 100Hz ripple. The seven-level output voltage v_{inva} can be seen in Fig. 14(c), which is a 7-level voltage with CPS-PWM.

In order to verify the effectiveness of the RPRA, the output power of the second inverter module maintains 360W and the other modules decrease to 240W. Fig. 15 shows experimental waveforms with an imbalanced power generation. The THD of the grid current is 7.1%, which is shown in Fig. 15(a). The inverter module output voltages can be seen in Fig. 15(b), where the output voltage of the second module v_{h2a} is kept at a steady value during many PWM periods and is different

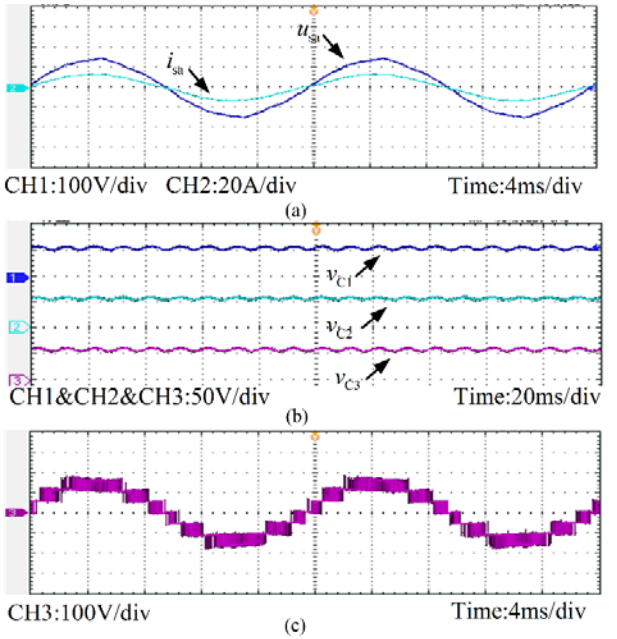

Fig. 14. Experimental waveforms for a CHB grid-connect PV system with balanced power generation: (a) grid voltage v_{sa} and grid current i_{sa}; (b) three capacitance voltages; (c) converter output voltage v_{inva}.

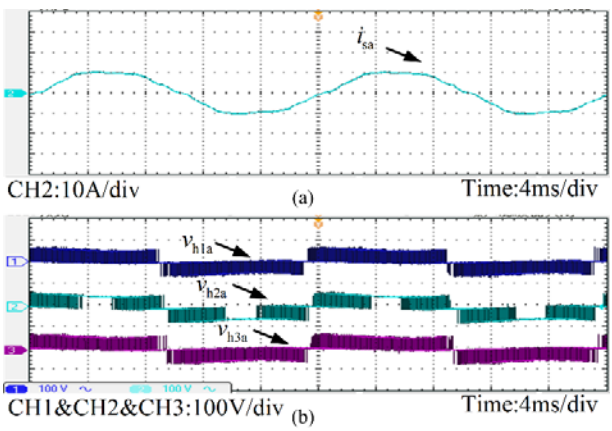

Fig. 15. Experimental waveforms for a CHB grid-connect PV system under unsymmetrical active power generation without the proposed strategy: (a) grid current i_{sa}; (b) module output voltage v_{hia}.

from others. This waveform is similar to the one in Fig. 9.Then RPCA is embed in the control system (i_q^*=-5.7A) and RPRA is activated when over-modulation is detected. With the help of reactive power and RPCA, the THD of the grid current decreases to 5.1% (Fig. 16(b)) from 7.1% (Fig. 16(a)). The inverter module index with the maximum modulation amplitude M_{max} is 2, and the minimum modulation amplitude M_{min} is equal to 1 or 3 to form the combination with the second inverter module as shown in Fig. 16(d). The output voltage waveforms of the three modules v_{h1a}, v_{h2a} and v_{h3a} are shown in Fig. 16(c). It can be seen that the proposed strategy mitigates over-modulation by comparing the waveforms v_{h2a} in Fig. 15 and v_{h2a} in Fig. 16.

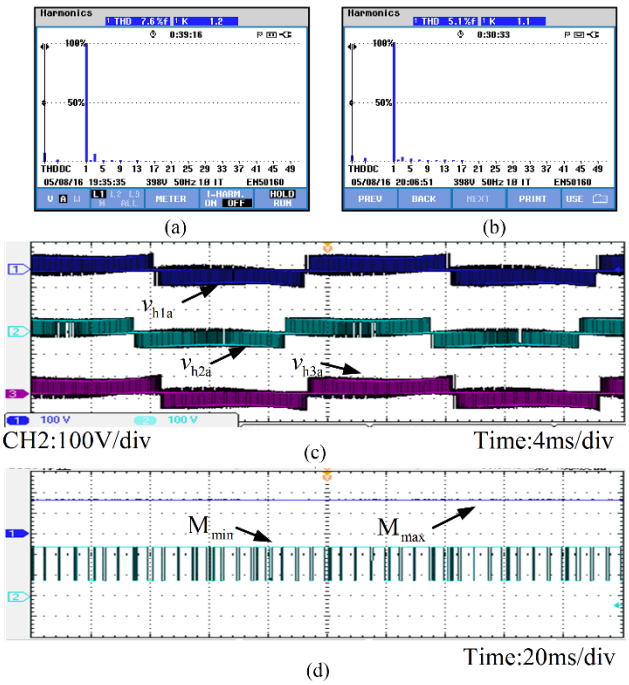

Fig. 16. Experimental waveforms for a CHB grid-connect PV system under unbalanced power conditions with the proposed strategy. (a) Grid current THD without the proposed strategy under an unbalanced output power. (b) Grid current THD with the proposed strategy. (c) Module output voltage v_{hia}. (d) Inverter module index with the maximum modulation amplitude M_{max} and the minimum modulation amplitude M_{min}.

VI. Conclusion

This paper has presented a dynamic power redistribution strategy for CHB PV systems to address the over-modulation caused by unbalanced power generation. With the proposed strategy, the control system can make the best of the dynamical redistribution of q-axis duty cycles and keep the system operating stably with an inter-bridge power imbalance.

The ability to eliminate over-modulation is limited by the reactive current factor and the inter-module power imbalance indicator, which is derived in this paper. In addition, simulation and experimental results are presented to verify the validity of RPRA.

References

[1] European Photovoltaic Industry Association, *Global Market Outlook for Photovoltaics 2016-2020*, 2016.

[2] S. Kouro, J. I. Leon, D. Vinnikov, and L. G. Franquelo, "Grid-connected photovoltaic systems: An overview of recent research and emerging PV converter technology," *IEEE Ind. Electron. Mag.*, Vol. 9, No. 1, pp. 47-61, Mar. 2015.

[3] J. Sastry, P. Bakas, H. Kim, L. Wang, and A. Marinopoulos, "Evaluation of cascaded h-bridge inverter for utility-scale photovoltaic systems," *Renew. Energy*, Vol. 69, pp.208-218, Sep. 2014.

[4] S. Kouro, M. Malinowski, K. Gopakumar, J. Pou, and L. G. Franquelo, "Recent advances and industrial applications of multilevel converters," *IEEE Trans. Ind. Electron.*, Vol. 57, No. 8, pp. 2553-2580, Aug. 2010.

[5] W. Zhao, H. Choi, G. Konstantinou, M. Ciobotaru, and V. G. Agelidis, "Cascaded h-bridge multilevel converter for large-scale PV grid-integration with isolated DC-DC stage," in *Power Electronics for Distributed Generation Systems (PEDG), 2012 3rd IEEE International Symposium on*, pp. 849-856, 2012.

[6] Y. Zhou and H. Li, "Analysis and suppression of leakage current in cascaded-multilevel-inverter-based PV systems," *IEEE Trans. Power Electron.*, Vol. 29, No. 10, pp. 5265-5277, Oct. 2014.

[7] P. Sochor and H. Akagi, "Theoretical comparison in energy-balancing capability between star- and delta-configured modular multilevel cascade inverters for utility-scale photovoltaic systems," *IEEE Trans. Power Electron.*, Vol. 31, No. 3, pp. 1980-1992, Mar. 2016.

[8] Y. Yu, G. Konstantinou, B. Hredzak, and V. G. Agelidis, "Operation of cascaded h-bridge multilevel converters for large-scale photovoltaic power plants under bridge failures," *IEEE Trans. Industrial Electron.*, Vol. 62, No. 11, pp. 7228-7236, Nov. 2015.

[9] C. D. Townsend, Y. Yu, G. Konstantinou and V. G. Agelidis, "Cascaded h-bridge multilevel PV topology for alleviation of per-phase power imbalances and reduction of second harmonic voltage ripple," *IEEE Trans. Power Electron.*, Vol. 31, No. 8, pp. 5574-5586, Aug. 2016.

[10] Y. Yu, G. Konstantinou, B. Hredzak, and V. G. Agelidis, "Power balance optimization of cascaded h-bridge multilevel converters for large-scale photovoltaic integration," *IEEE Trans. Power Electron*, Vol. 31, No. 2, pp. 1108-1120, Feb. 2016.

[11] J. Chavarria, D. Biel, F. Guinjoan, C. Meza, and J. J. Negroni, "Energy-balance control of PV cascaded multilevel grid-connected inverters under level-shifted and phase-shifted PWMs," *IEEE Trans. Ind. Electron.*, Vol. 60, No. 1, pp. 98-111, Jan. 2013.

[12] M. Coppola, F. Di Napoli, P. Guerriero, D. Iannuzzi, S. Daliento, and A. Del Pizzo, "An FPGA-based advanced control strategy of a grid-tied PV CHB inverter," *IEEE Trans. Power Electron.*, Vol. 31, No. 1, pp. 806-816, Jan. 2016.

[13] E. Villanueva, P. Correa, J. Rodriguez, and M. Pacas, "Control of a single-phase cascaded H-bridge multilevel inverter for grid-connected photovoltaic systems," *IEEE Trans. Ind. Electron.*, Vol. 56, No. 11, pp. 4399-4406, Nov. 2009.

[14] B. Xiao, L. Hang, J. Mei, C. Riley, L. M. Tolbert, and B. Ozpineci, "Modular cascaded h-bridge multilevel PV inverter with distributed MPPT for grid-connected applications," *IEEE Trans. Ind. Appl.*, Vol. 51, No. 2, pp. 1722-1731, Mar. 2015.

[15] Q. Huang, W. Yu, and A. Q. Huang, "Independent DC link voltage control of cascaded multilevel PV inverter," in *Proc 2016 APEC*, pp. 2727-2734, 2016.

[16] A. Eskandari, V. Javadian, H. Iman-Eini, and M. Yadollahi, "Stable operation of grid connected cascaded h-bridge inverter under unbalanced insolation conditions," in *Proc. EPECS*, pp. 1-6, 2013.

[17] M. Miranbeigi and H. Iman-Eini, "Hybrid modulation technique for grid-connected cascaded photovoltaic systems," *IEEE Trans. Ind. Electron.*, Vol. 63, No. 12, pp. 7843-7853, Dec. 2016.

[18] L. Liu, H. Li, Y. Xue, and W. Liu, "Decoupled active and reactive power control for large-scale grid-connected photovoltaic systems using cascaded modular multilevel converters," *IEEE Trans. Power Electron.*, Vol. 30, No. 1, pp. 176-187, Jan. 2015.
[19] L. Liu, H. Li, Y. Xue, and W. Liu, "Reactive power compensation and optimization strategy for grid-interactive cascaded photovoltaic systems," *IEEE Trans. Power Electron.*, Vol. 30, No. 1, pp. 188-202, Jan. 2015.
[20] Thin-film Terrestrial Photovoltaic (PV) Modules-Design Qualification and Type Approval, IEC61646, 2008
[21] H. Choi, W. Zhao, M. Ciobotaru, and V. Agelidis, "Large-scale PV system based on the multiphase isolated dc/dc converter," in *Proc. IEEE PEDG 2012*, pp. 801–807, 2012.
[22] J. Echeverria, S. Kouro, M. Perez, and H. Abu-Rub, "Multi-modular cascaded dc-dc converter for hvdc grid connection of large-scale photovoltaic power systems," in *Proc. IEEE IECON 2013*, pp. 6999–7005, 2013.
[23] S. Xu, A. Q. Huang, T. Zhao, and G. Wang, "Coupling effect reduction of a voltage-balancing controller in single-phase cascaded multilevel converters," *IEEE Trans. Power Electron.*, Vol. 27, No. 8, pp. 3530-3543, Aug. 2012.

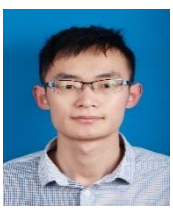

Kangan Wang was born in Jiangsu, China, on June 5, 1990. He received his B.S. degree in Electrical Engineering from China University of Mining and Technology, Xuzhou, China, where he is presently working towards his Ph.D. degree in Electrical Engineering. His current research interests include cascaded H-bridge multilevel converters and dc-dc converter topologies.

Xiaojie Wu received his B.S. degree in Industrial Automation, and his M.S. and Ph.D. degrees in Electrical Engineering from China University of Mining and Technology, Xuzhou, China, in 1988, 1991 and 2000, respectively. From 2002 to 2004, he was a Postdoctoral Research Fellow with Tsinghua University, Beijing. China. Since 1991, he has been with the School of Information and Electrical Engineering, China University of Mining and Technology, where he is presently working as a Professor. He has authored or coauthored 1 book and more than 60 technical papers published in journals and conference proceedings. His current research interests include advanced control of electrical drives, multilevel converters, renewable energy generation systems, and power electronics.

Fujin Deng received his B.S. degree in Electrical Engineering from China University of Mining and Technology, Xuzhou, China, in 2005; his M.S. degree in Electrical Engineering from Shanghai Jiao Tong University, Shanghai, China, in 2008; and his Ph.D. degree in Energy Technology from the Department of Energy Technology, Aalborg University, Aalborg, Denmark, in 2012. He joined the Southeast University, Nanjing, China, in 2017, where he is presently working as a Professor in the School of Electrical Engineering, Southeast University, Nanjing, China. From 2013 to 2015 he was a Postdoctoral Researcher and from 2015 to 2017 he was an Assistant Professor in the Department of Energy Technology, Aalborg University, Aalborg, Denmark. His current research interests include wind power generation, multilevel converters, high-voltage direct-current (HVDC) technologies, DC grids, and offshore wind farm-power system dynamics.

Feng Liu was born in Jiangsu, China, on January 2, 1991. He received his B.S. degree from Heilongjiang University of Science and Technology, Harbin, China. He is presently working towards his M.S. degree in Electrical Engineering at China University of Mining and Technology, Xuzhou, China. His current research interests include the topologies and control of dc-dc converters.